

**EXPLORING THE POTENTIAL OF PLANT SECONDARY  
METABOLITES FOR THEIR ANTIBIOTIC POTENTIATING ACTIVITY  
AGAINST MULTI-DRUG RESISTANT BACTERIA**

**BHANI KONGKHAM**



**CENTRE FOR RURAL DEVELOPMENT AND TECHNOLOGY  
INDIAN INSTITUTE OF TECHNOLOGY DELHI  
AUGUST 2024**

© Indian Institute of Technology Delhi (IITD), New Delhi, 2024

**EXPLORING THE POTENTIAL OF PLANT SECONDARY  
METABOLITES FOR THEIR ANTIBIOTIC POTENTIATING  
ACTIVITY AGAINST MULTI-DRUG RESISTANT BACTERIA**

by

**BHANI KONGKHAM**

**CENTRE FOR RURAL DEVELOPMENT & TECHNOLOGY**

submitted

in fulfillment of the requirements of degree of Doctor of Philosophy

to the

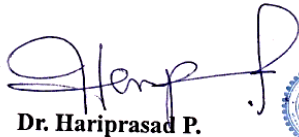


**INDIAN INSTITUTE OF TECHNOLOGY DELHI**

**AUGUST 2024**

## CERTIFICATE

This is to certify that the thesis entitled, “Exploring the potential of plant secondary metabolites for their antibiotic potentiating activity against multi-drug resistant bacteria”, being submitted by Ms. Bhani Kongkham to the Indian Institute of Technology Delhi for the award of “Doctor of Philosophy” is a record of bonafide research work carried out by her. She has worked under my guidance and supervision and has fulfilled the requirement for the submission of this thesis. To the best of my knowledge, the results obtained in this thesis has not been submitted in part or full to any other university or institute for the award of any degree or diploma.



**Dr. Hariprasad P.**



**Dr. HARIPRASAD P.**  
Associate Professor  
Centre for Rural Development & Technology  
Indian Institute of Technology Delhi  
Hauz Khas, New Delhi-110016, INDIA

Associate Professor

Centre for Rural Development and Technology

Indian Institute of Technology Delhi

New Delhi-110016

## ACKNOWLEDGEMENTS

As I write this acknowledgment page, I am filled with complex emotions. My heart is filled with gratitude as I remember all the people who have made this thesis possible.

I would like to start by acknowledging the Almighty, the supreme power in whose grace the world runs. Without his grace and kindness this journey will be impossible. I am reminded of His presence every day, and this feeling alone gives me enough strength to continue the mundane everyday life.

I am forever grateful to my supervisor, Prof. Hariprasad P. for his abled guidance throughout the PhD. The challenges given by him during this journey enabled me to develop a better understanding not only of research but of life in general. I now understand the idea that the shortest and easiest path is often not the best path. Success demands sacrifices, and each one of us is successful in our own ways and terms.

I am grateful to my SRC members, Prof. Anushree Malik, Prof. Pooja Ghosh, Prof. Shivaji Rao Gholap for their continuous support and guidance throughout my research work. My sincere thanks to CRC chairperson, Prof. VM Chariar, all faculties, and staff members of the Centre for Rural Development and Technology for providing facilities to carry out my research work. I am also thankful to the Director, Indian Institute of Technology Delhi for providing me the infrastructure and advanced research facilities. Further, I am grateful to the research facilities provided by Central Research Facility and Nanoscale Research Facility, IIT Delhi, Central Drug Research Institute, Lucknow, and Sophisticated Analytical Instrument Facility, IIT Bombay. Additionally, I am also grateful to the University Grants Commission, Govt. of India, for providing the JRF and SRF fellowships during my PhD.

I wish to extend my regards to my lab colleagues Mr. Ajay Yadav, Mrs. Monu Dinesh Ojha, Mr. Kapil, Ms. Anjali Gautam, Ms. Shazia Sheriff, Ms. Priyanka Ghelot, Ms. Leena Chouhan, Ms. Shivangini Panwar, Ms. Lemanaro Jamir, and Ms. Jaya Lakshmi for their support and well wishes during my PhD work. I am also thankful to Mr. Hridayaram for his help in the management of lab work. I also extend my gratitude to non-teaching staff of the institute, Mrs. Joshi, Mrs. Pratibha Rana, Mr. Rajendar, and Mr. Chopra for helping me in handling and processing of my official documents. I would also like to thank all my well-wishers whom I may have forgotten to mention.

The source of my energy apart from myself (default), will be my friends who are my well-wishers and people whose eyes shine when I succeed. I am forever thankful to my friend “Dr. Pankaj Kumar” who has been there throughout my journey. The exchange of ideas and insightful communications I had with him was a blessing when things were tough. I am also grateful to my dearest friend, “Dr. Shafali Garg” and her family who has always made me feel the presence of a family in Delhi. Her warmth and kindness precede her reputation, she is like the sunshine in a rainy day.

I believe that I am blessed, as I found a friend and mentor in my senior, “Dr. Duraivadivel P” who patiently listened to my problems when I was a fresher in the lab. His calm and patient nature taught me a different aspect of life. Without his support I would have been a lone warrior. I wholeheartedly thank him for being a very helpful co-author of my publications and for being my 3 a.m. friend.

I dedicate my thesis to my father, “Mr. Kongkham Bhimo Singh” and my late mother, “Mrs. Kongkham Basanti Devi” for all the faith, support, trust, and freedom they have given me. I believe that the biggest gift one could get is the gift of freedom and time. I am also thankful to my sister, “Kongkham Bideshori Devi” who has stood like a pillar for the family in tough times. Her contribution to the family enabled me to get all the freedom and time required for the PhD. I am thankful to my brother, “Kongkham Bhupendra Singh” and my elder sister, “Kongkham Bidyapati Devi” for their support and good wishes. Lastly, I am grateful to the biggest entertainer (3-year-old) of the family, “Gugu” for his giggles and funny gibberish words.

Best Wishes

Bhani Kongkham

## Abstract

Since time immemorial plant extracts have been used for their antibacterial properties. In recent time, the active compounds have been isolated and their activities are established. However, considering the diversity of the plant kingdom and their secondary metabolites, further research needs to be done to identify potential metabolites having direct antibacterial and antibiotic potentiation ability. The identification of antibiotic potentiators is important considering the rapid development of bacterial resistance against the antibiotics thereby depleting the antibiotic pipeline. To address this issue of bacterial resistance and to find antibiotic potentiating plant metabolites, the present study was carried out under four objectives.

High throughput method was employed for screening of 180 extracts in different solvents obtained from 30 plants. These extracts were screened for  $\beta$ -lactamase inhibition and  $\beta$ -lactam potentiation ability against the MDR bacterial isolates (*Escherichia coli*, *Pseudomonas aeruginosa*, *Acinetobacter baumannii*, and *Bacillus cereus*). Among the extracts, acetone extract of *Ficus religiosa* and hexane extract of *Acorus calamus* was found to be the most effective in terms of  $\beta$ -lactamase inhibition and ampicillin potentiation.

The metabolites present in *F. religiosa* were identified using HR-LCMS. Further, to understand the binding of the metabolites with Class A  $\beta$ -lactamases (TEM 1, SHV1, KPC-2 and 6D17) molecular docking and MD simulation studies were performed. This revealed that taxifolin and miquelianin showed the best binding affinity with all the four class A  $\beta$ -lactamases. Hydrogen bond occupancy of >200 % was seen with Glu166, Glu240, Asn132, etc. which are located in the enzyme active site. Additionally, the ADMET profile of the metabolites showed their drug likeliness and non-toxic nature.

Fractionation of bioactive compounds from *A. calamus* rhizome hexane (AC-R-H) extract was performed and its MIC, FIC index and mode of action was determined. AC-R-H bioactive fraction was found to reduce the MIC of ampicillin against *E. coli* (100 mg/mL to 25 mg/mL), *P. aeruginosa* (15 mg/mL to 3.25 mg/mL), *A. baumannii* (12.5 mg/mL to 1.56 mg/ml), and *B. cereus* (10 mg/mL to 1.25 mg/mL). Further it recorded synergistic activity with ampicillin against *B. cereus* (FICI = 0.365), *P. aeruginosa* (FICI = 0.456), and *A. baumannii* (FICI = 0.364). This activity can be attributed to its ability to alter the fatty acid composition of the bacterial cell membranes, hinder the membrane integrity, permeability, and cause cell membrane damage. It also showed good antibiofilm activity against *B. cereus* and a moderate  $\beta$ -lactamase inhibition ( $IC_{50}$  = 6.2 mg/mL). Characterization of AC-R-H bioactive fraction through UV-Vis, FT-IR, and GC-MS revealed Asarone as the major compound present in the bioactive fraction.

Finally, PLGA based formulation was prepared by encapsulating the clarified crude of *A. calamus*. The encapsulated particles exhibited size (300-500 nm), PDI (0.3-0.4) and zeta potential (-25 to -15 mV). The loading capacity and encapsulation efficiency of the particles were (40 to 60 %) and *in vitro* release profile showed burst release with ~70 % of cumulative release in 24 h. The encapsulated particles showed antibacterial efficacy and ampicillin potentiation against *A. baumannii*. Further, the cell toxicity studies of clarified crude and encapsulated particles (20  $\mu$ g/ml) on Vero cells showed ~20 % inhibition. Overall, the study identifies two plants *F. religiosa* and *A. calamus* and their metabolites as potential candidates for countering multidrug resistance in bacteria. Also, the development of PLGA based formulation encapsulating *A. calamus* clarified crude showcases the feasibility to develop biocompatible formulation with multiple compounds.

## सार

प्राचीन काल से वनस्पतियों के अर्क/सत्त का उपयोग उनके एंटीबैक्टीरियल गुणों के लिए किया जाता रहा है। हाल के समय में, उन वनस्पतियों के अर्क/सत्त से सक्रिय यौगिकों को अलग कर उनकी कार्यलाप को समझने की कोशिश की गई है। हालाँकि, सृष्टि जगत के वनस्पतियों और उनके द्वितीयक मेटाबोलाइट्स की विविधता को ध्यान में रखते हुए, प्रत्यक्ष एंटीबैक्टीरियल और एंटीबायोटिक सामर्थ्य वाले संभावित मेटाबोलाइट्स की पहचान करने के लिए और अधिक शोध किए जाने की आवश्यकता है। इसके अतिरिक्त, बैक्टीरिया के प्रतिरोध क्षमता में तेजी से विकास के कारण असरदार एंटीबायोटिक दवाओं की उपलब्धता में तेजी से कमी आने को ध्यान में रखते हुए नए एंटीबायोटिक सामर्थ्य वाले संभावित मेटाबोलाइट्स की खोज महत्वपूर्ण है। इसलिए, बैक्टीरिया के बढ़ते प्रतिरोध क्षमता से उत्पन्न परिस्थिति के समाधान करने और नए एंटीबायोटिक सामर्थ्य वाले संभावित मेटाबोलाइट्स को खोजने के लिए, वर्तमान अध्ययन को चार उद्देश्यों के तहत किया गया।

30 पौधों से प्राप्त 180 अर्क/सत्त की विभिन्न विलायकों में उच्च थ्रूपुट विधि के द्वारा जाँच किया गया। एमडीआर बैक्टीरियल आइसोलेट्स (*एस्चेरिचिया कोली*, *स्यूडोमोनस एरुगिनोसा*, *एसिनेटोबैक्टर बाउमन्नी* और *बैसिलस सेरिअस*) के प्रति  $\beta$ -लैक्टामेज़ नियंत्रण और  $\beta$ -लैक्टम सामर्थ्यता के लिए इन अर्कों/सत्तों की जांच की गई। इनमें से, *फाइकस रिलिजियोसा* के एसीटोन अर्क और *एकोरस कैलामस* के हेक्सेन अर्क को  $\beta$ -लैक्टामेज़ नियंत्रण और एम्पीसिलीन सामर्थ्यता के मामले में सबसे प्रभावी पाया गया।

*फाइकस रिलिजियोसा* में मौजूद मेटाबोलाइट्स की पहचान एचआर-एलसीएमएस का उपयोग करके किया गया। इसके अलावा, श्रेणी ए  $\beta$ -लैक्टामेस (टीईएम-1, एसएचवी-1, केपीसी-2 और 6डी17) के साथ मेटाबोलाइट्स के आबंधन को समझने के लिए आणविक डॉकिंग और एमडी सिमुलेशन अध्ययन किए गए। इससे पता चला कि टैक्सीफोलिन और मिकेलियानिन के चार श्रेणी ए  $\beta$ -लैक्टामेस के साथ सबसे अच्छा आबंधन होता है। एंजाइम सक्रिय साइट में अवस्थित ग्लू-166, ग्लू-240, एसएन-132, इत्यादि में 200% से भी अधिक हाइड्रोजन बांड अधिभोग देख गया। इसके अतिरिक्त, मेटाबोलाइट्स के एडीएमईटी प्रोफाइल से उनकी गैर-विषाक्त प्रकृति और दवाई बनाने की संभावनाओं का भी पता चला।

*एकोरस कैलामस* राइजोम हेक्सेन (एसी-आर-एच) अर्क से बायोएक्टिव यौगिकों का अंशांकन करने के बाद इसके एमआईसी, एफआईसी सूचकांक और क्रियान्वयन के तरीके का निर्धारित किया गया। एसी-आर-एच बायोएक्टिव अंश *एस्चेरिचिया कोली* (100 मिलीग्राम/एमएल से 25 मिलीग्राम/एमएल), *स्यूडोमोनस एरुगिनोसा* (15 मिलीग्राम/एमएल से 3.25 मिलीग्राम/एमएल),

एसिनेटोबैक्टर बाउमन्नी (12.5 मिलीग्राम/एमएल से 1.56 मिलीग्राम/एमएल), और बैसिलस सेरिअस (10 मिलीग्राम/एमएल से 1.25 मिलीग्राम/एमएल) के एम्पीसिलीन के एमआईसी को कम करने के लिए उपयुक्त पाया गया। इसके अतिरिक्त, बैसिलस सेरिअस (एफआईसीआई = 0.365), स्ट्रुडोमोनस एरुगिनोसा (एफआईसीआई = 0.456), और एसिनेटोबैक्टर बाउमन्नी (एफआईसीआई = 0.364) के प्रति एसी-आर-एच अर्क का एम्पीसिलीन के साथ सहक्रियात्मक गतिविधि का भी पता चला। इस गतिविधि को बैक्टीरिया कोशिका झिल्ली की फैटी एसिड संरचना को बदलने, झिल्ली की संपूर्णता और पारगम्यता में बाधा डालने और कोशिका झिल्ली को नुकसान पहुंचाने की क्षमता से सम्बद्ध किया जा सकता है। एसी-आर-एच अर्क ने बैसिलस सेरिअस के प्रति अच्छी एंटीबायोफिल्म गतिविधि और मध्यम  $\beta$ -लैक्टामेज़ नियंत्रण ( $IC_{50} = 6.2$  मिलीग्राम/एमएल) भी दिखाया। एसी-आर-एच बायोएक्टिव अंश के यूवी-विज़, एफटी-आईआर और जीसी-एमएस निरूपण के माध्यम से बायोएक्टिव अंश में मौजूद प्रमुख यौगिक असारों का पता चला।

अंततः, एकोरस कैलामस के क्लारिफाइड क्रूड को संपुटित करके पीएलजीए आधारित फॉर्मूलेशन तैयार किया गया। एनकैप्सुलेटेड कणों का आकार (300-500 एनएम), पीडीआई (0.3-0.4), जीटा क्षमता (-25 से -15 एमवी), लोडिंग क्षमता और एनकैप्सुलेशन दक्षता (40 से 60%) प्राप्त हुआ। इन-विट्रो रिलीज़ प्रोफाइल से पता चला कि बस्ट रिलीज़ 24 घंटों में संचयी रिलीज़ का लगभग 70% होता है। एनकैप्सुलेटेड कणों में एसिनेटोबैक्टर बाउमन्नी के प्रति एंटीबैक्टीरियल गुण और एम्पीसिलीन सामर्थ्यता का पता चला। इसके अलावा, वेरो कोशिकाओं पर क्लारिफाइड क्रूड और एनकैप्सुलेटेड कणों (20 माइक्रोग्राम/एमएल) के कोशिका विषाक्तता अध्ययन में लगभग 20% विनियंत्रण का पता चला। कुल मिलाकर, अध्ययन में बैक्टीरिया के मल्टीड्रग प्रतिरोध का मुकाबला करने के लिए संभावित दो पौधों फाइकस रिलिजियोसा और एकोरस कैलामस और उनके मेटाबोलाइट्स का पता चला। इसके अलावा, एकोरस कैलामस क्लारिफाइड क्रूड को समाहित करने वाले पीएलजीए आधारित फॉर्मूलेशन का विकास कई यौगिकों के साथ जैव-संगत फॉर्मूलेशन विकसित करने की व्यवहार्यता को दर्शाता है।

## TABLE OF CONTENTS

<b>Certificate</b>	i
<b>Acknowledgements</b>	ii-iii
<b>Abstract</b>	iv-vii
<b>Table of contents</b>	viii-x
<b>List of figures</b>	xi-xvi
<b>List of tables</b>	xvii
<b>List of abbreviations</b>	xviii-xix
<b>Chapter 1: Introduction</b>	21-34
<b>Chapter 2: Review of Literature</b> 2.1 Introduction 2.2 Chemical nature and mode of action of PSMs 2.2.1. Inhibitors of modified active site 2.2.2. Inhibitors of enzymes that inactivate drugs 2.2.3. Bacterial cell membrane disruption and permeability enhancements 2.2.4. Bacterial cellular metabolism impairment 2.2.5. Inhibitors of efflux pumps 2.2.6. Interruption of DNA/RNA and protein synthesis 2.2.7. Disruption of quorum sensing and anti-biofilm activity 2.2.8. Inhibiting bacterial capsule production 2.3. <i>In vivo</i> studies using PSMs alone or in combination with antibiotics 2.4. <i>In-silico</i> studies on combinatorial therapy against antibiotic resistant bacteria 2.5. Hurdles and strategies in the commercialisation of PSMs 2.6. Safety issues while using plant secondary metabolites 2.7. Priority areas of research 2.8. Conclusion 2.9. Research gap 2.10. Objectives	35-64
<b>Chapter 3: High throughput screening of plant extracts for <math>\beta</math>-lactamase inhibition and <math>\beta</math>-lactam potentiation targeting antibiotic resistant bacteria</b> 3.1 Introduction 3.2 Material and Methods 3.2.1 Plant sample collection, processing, and extraction 3.2.2 Bacteria culture collection and maintenance 3.2.3 Bacterial antibiotic resistance/susceptibility pattern determination 3.2.4 Bacterial growth curve and ampicillin IC <sub>50</sub> concentration determination 3.2.5 Bacterial characterisation 3.2.5.1 Determination of bacterial $\beta$ -lactamase production 3.2.5.2 Determination of bacterial biofilm production 3.2.5.3 Determination of bacterial siderophore production 3.2.5.4 Determination of bacterial protease production 3.2.5.5 Bacterial motility test 3.2.6 <i>In vitro</i> screening of plant extracts for $\beta$ -lactamase inhibition 3.2.7 <i>In vitro</i> screening of plant extracts for ampicillin potentiation assay 3.3 Statistical analysis 3.4 Results and Discussion 3.4.1 Bacterial characterization 3.4.2 The $\beta$ -lactamase inhibition ability of plant extracts	65-82

3.4.3 Antibacterial and ampicillin potentiating activity of plant extracts	
3.5 Conclusion	
<b>Chapter 4: Purification of antibiotic potentiating plant secondary metabolites from <i>Acorus calamus</i> rhizome and understanding their mode of action against MDR bacteria</b> 4.1 Introduction 4.2 Materials and methods 4.2.1 Checkerboard assay 4.2.2 Assay guided fractionation of <i>Acorus calamus</i> rhizome hexane extract 4.2.2.1 Thin layer chromatography (TLC) 4.2.2.2 TLC agar overlay autobiography technique 4.2.2.3 Separation of bioactive fraction using column chromatography 4.2.3 GC-MS, UV-Vis spectral scanning, and FT-IR analysis 4.2.4 Mechanism of action of active compounds 4.2.4.1 Bacterial membrane damage analysis through SEM 4.2.4.2 Alteration of bacterial membrane permeability 4.2.4.2.1 Proteins and carbohydrate leakage 4.2.4.2.2 SYBR Green I and propidium iodide assay 4.2.4.3 EtBr accumulation assay for determining efflux pump inhibition. 4.2.4.4 $\beta$ -lactamase inhibition assay 4.2.4.5 Inhibition of bacterial biofilm formation 4.2.4.6 Determination of the effect of treatment with the purified fraction on the fatty acid composition of bacteria using GC-FAME analysis 4.2.4.7 Determination of bacterial cell viability using MTT dye 4.3 Statistical analysis 4.4 Result and Discussion 4.4.1 <i>Acorus calamus</i> L. rhizome extract exhibits antibacterial effect and potentiates ampicillin activity against MDR bacteria. 4.4.2 Purification of bioactive fraction from <i>A. calamus</i> rhizome hexane extract 4.4.3 Determination of compounds present in the bioactive fraction. 4.4.4 Stage-III bioactive fraction potentiates the function of ampicillin 4.4.5 Determination of bacterial viability after treatment with stage-III bioactive fraction 4.4.6 Elucidating the mode of action of stage-III bioactive fraction 4.4.6.1 Membrane damage and permeability alteration analysis 4.4.6.1.1 Morphological analysis through SEM 4.4.6.1.2 SYBR green I and PI assay 4.4.6.1.3 Protein and carbohydrate leakage assay 4.4.6.2 Biofilm inhibition assay using crystal violet dye 4.4.7 Determination of $\beta$ -lactamase inhibition and efflux pump inhibition ability 4.4.8 Changes in bacterial cell membrane fatty acid composition exposed to bioactive fraction (S-III-BAF) 5. Conclusion	83-134
<b>Chapter 5: Analyzing <math>\beta</math>-lactamase inhibitory plant secondary metabolites in <i>Ficus religiosa</i> through HR-LCMS and <i>in silico</i> studies</b> 5.1. Introduction 5.2. Materials and methods 5.2.1 Metabolite library preparation of <i>Ficus religiosa</i>	135-192

<p>5.2.2 Ensemble molecular docking and structure-activity relationship analysis of ligands</p> <p>5.2.3 Molecular dynamics simulations and data analysis</p> <p>5.2.4 MMPBSA free binding energy analysis</p> <p>5.2.5 Pharmacokinetics and ADMET profiles</p> <p>5.3 Results and Discussion</p> <p>5.3.1 Ensemble docking and structure-activity relationship analysis.</p> <p>5.3.2 MD simulation studies</p> <p>5.3.3 Pharmacokinetics and ADMET profiles of the molecules</p> <p>5.4 Conclusion</p>	
<p><b>Chapter 6: Encapsulation of bioactive fraction from <i>Acorus calamus</i> hexane extract and their efficacy analysis</b></p> <p>6.1. Introduction</p> <p>6.2. Materials and methods</p> <p>6.2.1 Extraction and GC-MS analysis of <i>A. calamus</i> bioactive fraction</p> <p>6.2.2. Antibacterial and ampicillin potentiation ability of <i>A. calamus</i> clarified crude.</p> <p>6.2.3. Optimization of conditions for PLGA based formulation preparation</p> <p>6.2.3.1. Preparation of <i>A. calamus</i> clarified crude encapsulated PLGA particles.</p> <p>6.2.3.2. Determination of loading capacity and encapsulation efficiency</p> <p>6.2.3.3. Particle size, distribution, and zeta potential characterization</p> <p>6.2.3.4. FTIR, FESEM, and TLC analysis of the particles</p> <p>6.2.4. <i>In vitro</i> release study</p> <p>6.2.5. Antibacterial and ampicillin potentiation study</p> <p>6.2.6. Cytotoxicity analysis of <i>A. calamus</i> clarified crude encapsulated formulation</p> <p>6.3. Statistical analysis</p> <p>6.4. Results and discussion</p> <p>6.4.1. Metabolites in clarified crude and antibacterial activity evaluation</p> <p>6.4.2. Clarified crude encapsulated particle preparation and characterization.</p> <p>6.4.3. Effect of drug-polymer ratio on the loading capacity and encapsulation efficiency.</p> <p>6.4.4. Determination of encapsulated particle chemical composition and morphology</p> <p>6.3.5. <i>In vitro</i> release study of clarified crude encapsulated particles</p> <p>6.4.5. Antibacterial and ampicillin potentiating activity of encapsulated particles</p> <p>6.4.6. Cell toxicity study of the clarified crude and encapsulated particles.</p> <p>6.5. Conclusion</p>	193-224
<b>Summary</b>	225-227
<b>Conclusion</b>	228-229
<b>Future Scope</b>	230
<b>References</b>	231-277
<b>Biodata</b>	278-279

## LIST OF FIGURES

Figure No.	Title of the Figure	Page No.
Fig. 2.1	Interaction of antibiotic and bacteria over time results in development of new resistant bacterial strains having different mechanisms of resistance. The use of PSMs along with antibiotics can help in countering this never-ending threat.	37
Fig. 2.2	Mechanistic basis of antibiotic resistance involves different routes. Combination of PSMs and conventional antibiotics is proposed to increase bacterial susceptibility and a possible solution to counter AMR.	51
Fig. 3.1	Bacterial isolates grown in nutrient agar plates.	74
Fig. 3.2	Soft agar assay for testing bacterial motility.	74
Fig. 3.3	Detection of bacterial siderophore production using CAS agar plates.	74
Fig. 3.4	Determination of bacterial $\beta$ -lactamase production using nitrocefin as substrate.	74
Fig. 3.5	Determination of bacterial biofilm production using crystal violet dye.	75
Fig. 3.6	Determination of bacterial protease production using azocasein as substrate.	75
Fig. 3.7	Growth curves of the four bacterial isolates.	76
Fig. 3.8	IC <sub>50</sub> value of ampicillin against the four bacterial isolates, measured at 15 h of incubation.	76
Fig. 3.9	Antibiotic resistance and susceptibility pattern of the four bacterial isolates determined using disc diffusion assay.	77
Fig. 3.10	Heat map indicating antibiotic resistance and susceptibility pattern of the four bacterial isolates, measured through disc diffusion assay.	78
Fig. 3.11	Clustered heat map presenting $\beta$ -lactamase inhibition potential of plant extracts represented as IC <sub>50</sub> (mg/ml).	80
Fig. 3.12	Heat map indicating bacterial growth inhibition in presence of plant extract alone and plant extract along with ampicillin combination.	82
Fig. 4.1	Assay guided purification flow chart of <i>A. calamus</i> rhizome hexane extract.	97
Fig. 4.2	TLC banding pattern of <i>Acorus calamus</i> rhizome hexane extract. A: visible light; B: short wave UV (254 nm); C: long wave UV (365 nm).	98
Fig. 4.3	TLC banding pattern of column chromatography fractions (six fractions named as F1 to F6). A: visible light; B: short wave UV (254 nm); C: long wave UV (365 nm).	98

Fig. 4.4	TLC autobiography assay of the column chromatography fractions (six fractions named as F1 to F6) against <i>Bacillus cereus</i> .	99
Fig. 4.5	Flash chromatogram of the bioactive fraction obtained from column chromatography. The red, purple, and orange peaks indicate the peaks detected at 254 nm, 280 nm, and 200-300 nm wavelengths.	99
Fig. 4.6	A-C: TLC banding pattern of flash chromatography fractions (48-51) in visible, short, and long UV light; D: TLC autobiography assay of the bioactive fraction (S-III-BAF) against <i>B. cereus</i> .	100
Fig.4.7	GC-MS chromatogram of the different stages of purification.	102
Fig. 4.8	GC-MS chromatogram of A: $\alpha$ -Asarone (standard) and B: $\beta$ -Asarone (standard).	103
Fig. 4.9	FTIR spectra of S-III-BAF.	103
Fig. 4.10	UV-vis spectral scan of S-III-BAF.	104
Fig. 4.11	A: FT-IR spectra and B: UV-Vis spectral scan of $\alpha$ -Asarone (standard).	104-105
Fig. 4.12	A: FT-IR spectra and B: UV-Vis spectral scan of $\beta$ -Asarone (standard).	106
Fig. 4.13	m/z spectra of major peak present in A: $\alpha$ -Asarone (standard); B: $\beta$ -Asarone (standard), and C: stage-III-bioactive fraction.	106
Fig. 4.14	Checkerboard assay performed using AC-R-H extract alone, S-III-BAF alone, and combination of either AC-R-H extract or S-III-BAF with ampicillin against <i>B. cereus</i> , <i>A. baumannii</i> , <i>P. aeruginosa</i> , and <i>E. coli</i> . A: 96 well plate after resazurin addition (real experimental image); B: <i>A. calamus</i> rhizome hexane extract bioactive fraction (S-III-BAF) and C: <i>A. calamus</i> rhizome hexane extract. Pink colour indicates wells where there is bacterial growth while blue colour indicates wells where there is no bacterial growth (MIC).	108-109
Fig. 4.15	Time kill assay of bacteria ( <i>Acinetobacter baumannii</i> , <i>Pseudomonas aeruginosa</i> , <i>Escherichia coli</i> , <i>Bacillus cereus</i> ) after treatment with T1 (control), T2 (ampicillin, AB), T3 (S-III-BAF), and T4 (ampicillin + S-III-BAF).	112
Fig. 4.16	A: SEM images of <i>Bacillus cereus</i> with and without treatments. B: SEM images of <i>Acinetobacter baumannii</i> with and without treatments. C: SEM images of <i>Pseudomonas aeruginosa</i> with and without treatments. D: SEM images of <i>Escherichia coli</i> with and without treatments.	113-115
Fig. 4.17	A: Effect of different treatments on membrane permeability of <i>B. cereus</i> determined using SYBR Green and PI dye and observed under confocal microscope (Scale: 10 $\mu$ m).	116-119

	B: Effect of different treatments on membrane permeability of <i>A. baumannii</i> determined using SYBR Green and PI dye and observed under confocal microscope (Scale: 10 $\mu$ m). C: Effect of different treatments on membrane permeability of <i>E. coli</i> determined using SYBR Green and PI dye and observed under confocal microscope (Scale: 10 $\mu$ m). D: Effect of different treatments on membrane permeability of <i>P. aeruginosa</i> determined using SYBR Green and PI dye and observed under confocal microscope (Scale: 10 $\mu$ m).	
Fig. 4.18	Leakage of protein and carbohydrate from bacterial cells exposed to different treatments.	121
Fig. 4.19	Biofilm inhibition in <i>Bacillus cereus</i> after treatments T1 (control); T2 (ampicillin, AB); T3 (S-III-BAF); T4 (S-III-BAF + ampicillin); T5 (AC-R-H); and T6 (AC-R-H + ampicillin) respectively.	122
Fig. 4.20	Linear regression curve for IC <sub>50</sub> determination of bioactive fraction (S-III-BAF) for $\beta$ -lactamase inhibition.	124
Fig. 4.21	Effect of A: <i>A. calamus</i> crude extract and B: bioactive fraction (S-III-BAF) on the accumulation of EtBr by <i>A. baumannii</i> .	124
Fig. 4.22	A: GC chromatogram of 37 component FAME mix standard. B: Chromatogram of the fatty acids detected in <i>B. cereus</i> treated and control samples using GC-FID analysis. C: Chromatogram of the fatty acids detected in <i>A. baumannii</i> treated and control samples using GC-FID analysis. D: Chromatogram of the fatty acids detected in <i>P. aeruginosa</i> treated and control samples using GC-FID analysis. E: Chromatogram of the fatty acids detected in <i>E. coli</i> treated and control samples using GC-FID analysis.	126-130
Fig. 4.23	Alteration in bacterial membrane fatty acid composition before and after treatments. The four treatments are T1 (control); T2 (ampicillin); T3 (S-III-BAF); and T4 (ampicillin + S-III-BAF).	131
Fig. 5.1	2-D interactions between the proteins SHV1, TEM1, CTX-M-27 and KPC-2 and ligands visualised using Discovery Studio software.	144-146
Fig. 5.2	Structure-activity relationship analysis of PSM showing BE of $\leq -5$ kcal/mol using Data warrior software.	146
Fig. 5.3	Structure of plant metabolites used for MD simulation study.	147
Fig. 5.4	A. RMSD, RMSF, SASA, Rg of SHV1 (PDB ID: 1SHV) and SHV1-ligand complex. B. RMSD, RMSF, SASA, Rg of TEM1 (PDB ID: 4OQG) and TEM1-ligand complex. C. RMSD, RMSF, SASA, and Rg of CTX-M-27 (PDB ID: 6BU3) and CTX-M-27 and ligand complex.	161-164

	D. RMSD, RMSF, SASA, and Rg of KPC-2 (PDB ID: 6D17) and KPC-2 and ligand interactions.	
Fig. 5.5	A. H-bond number formed during 50 ns MD simulation of TEM1-ligand complexes. B. H-bond number formed during 50 ns MD simulation of SHV1-ligand complexes. C. H-bond number formed during 50 ns MD simulation of CTX-M-27-ligand complexes. D. H-bond number formed during 50 ns MD simulation of KPC-2-ligand complexes.	165-168
Fig. 5.6	A. Hydrogen bond distance observed during the MD simulation of TEM1-ligand complex. B. Hydrogen bond distance observed during the MD simulation of SHV1-ligand complex. C. Hydrogen bond distance observed during the MD simulation of CTX-M-27-ligand complex. D. Hydrogen bond distance observed during the MD simulation of KPC-2-ligand complex.	169-172
Fig. 5.7	Molecular dynamics simulations data analysis. A: Heat map with dendrogram representing H-bond occupancy during the last 10 ns of simulation for all proteins. B: Stacked bar graph representing H-bond number formed during 50 ns of simulation for all proteins. C: Binding energy (kJ/mol) of protein-ligand complex calculated using MMPBSA method.	173
Fig. 5.8	A. Protein-ligand interactions visualised using PyMol software. a: SHV1-avibactam; b: TEM1-avibactam; c: CTX-M-27-avibactam; d: KPC-2-avibactam; e: SHV1-tazobactam; f: TEM1-tazobactam; g: CTX-M-27-tazobactam; h: KPC-2-tazobactam. B. Protein-ligand interactions visualised using PyMol software. a: SHV1-queracetin; b: TEM1-queracetin; c: CTX-M-27-queracetin; d: KPC-2-queracetin; e: SHV1-ampicillin; f: TEM1-ampicillin; g: CTX-M-27-ampicillin; h: KPC-2-ampicillin. C. Protein-ligand interactions visualised using PyMol software. a: SHV1-luteolin; b: TEM1-luteolin; c: CTX-M-27-luteolin; d: KPC-2-luteolin; e: SHV1-taxifolin; f: TEM1-taxifolin; g: CTX-M-27-taxifolin; h: KPC-2-taxifolin. D. Protein-ligand interactions visualised using PyMol software. a: SHV1-myricetin; b: TEM1-myricetin; c: CTX-M-27-myricetin; d: KPC-2-myricetin; e: SHV1-miquelianin; f: TEM1-miquelianin; g: CTX-M-27-miquelianin; h: KPC-2-miquelianin.	177-182
Fig. 5.9	SwissADME analysis of the metabolites and standards used for MD simulation study along with their corresponding bioavailability score (BSA).	188
Fig. 6.1	Steps of PLGA based formulation preparation. 1: PLGA is dissolved in DCM; 2: PVA (1 %) in water is kept in beaker	197

	to which PLGA in DCM is added dropwise while continuous stirring; 3: sonication is done by placing the beaker containing emulsion in ice water; 4: the sonicated emulsion is kept for stirring at 400 rpm for 3 h; 5: the particles are purified by centrifugation in 3 washing steps using DI water; 6: the purified particles are lyophilized by adding 2.5% of trehalose. A: PLGA based formulation prepared using this process.	
Fig. 6.2	A: GC-MS spectra of clarified crude; B: m/z spectrum of Asarone (major peak) present in clarified crude.	202
Fig. 6.3	Checkerboard assay using different concentrations of clarified crude and ampicillin against <i>Acinetobacter baumannii</i> . A: 96 well plate after resazurin addition (real experimental image); B: pictorial representation of the experiment.	203
Fig. 6.4	Size and PDI of PLGA 75:25 at different time of sonication.	205
Fig. 6.5	Zeta potential of PLGA 75:25 at different time of sonication.	205
Fig. 6.6	Size and PDI of PLGA 50:50 at different time of sonication.	206
Fig. 6.7	Zeta potential of PLGA 50:50 at different time of sonication.	206
Fig. 6.8	Size, PDI, and zeta potential of loaded and unloaded PLGA particles. A: Size and PDI of PLGA 75:25; B: Zeta potential of PLGA 75:25; C: Size and PDI of PLGA 50:50; D: Zeta potential of PLGA 50:50	208
Fig. 6.9	Calibration curve of different concentrations of clarified crude in presence of PLGA 75:25 and trehalose.	209
Fig. 6.10	Calibration curve of different concentrations of clarified crude in presence of PLGA 50:50 and trehalose.	210
Fig. 6.11	FTIR spectra of clarified crude.	212
Fig. 6.12	FTIR spectra of $\beta$ -Asarone (standard).	212
Fig. 6.13	FTIR spectra of unloaded PLGA 75:25 particles.	213
Fig. 6.14	FTIR spectra of clarified crude loaded and unloaded PLGA 75:25 particles.	213
Fig. 6.15	FTIR spectra of clarified crude loaded and unloaded PLGA 50:50 particles.	214
Fig. 6.16	TLC observed in visible and short UV (245 nm) light. A: clarified crude; B: PLGA 75:25 unloaded; C: clarified crude loaded PLGA 75:25; D: clarified crude; E: PLGA 50:50 unloaded; F: clarified crude loaded PLGA 50:50.	214
Fig. 6.17	FESEM images of PLGA particles loaded and unloaded. A: PLGA 75:25 unloaded; B: PLGA 75:25 loaded; C: PLGA 50:50 unloaded; D: PLGA 50:50 loaded.	215
Fig. 6.18	Calibration curve of PBS+10% DMSO and clarified crude in different concentrations.	216
Fig. 6.19	<i>In vitro</i> drug release percentage of encapsulated PLGA 75:25 particles.	217
Fig. 6.20	<i>In vitro</i> cumulative release (%) of encapsulated PLGA 75:25 particles.	217
Fig. 6.21	<i>In vitro</i> drug release percentage of encapsulated PLGA 50:50 particles.	218

Fig. 6.22	<i>In vitro</i> cumulative release (%) of encapsulated PLGA 50:50 particles.	218
Fig. 6.23	<i>Acinetobacteria baumannii</i> cells viability measured using MTT dye at different time interval of incubation after treatment with different concentrations of encapsulated PLGA 75:25 particles and ampicillin.	220
Fig. 6.24	<i>Acinetobacter baumannii</i> cells viability percentage measured at 18 h of incubation after treatment with formulation alone and in combination with ampicillin.	222
Fig. 6.25	Percentage inhibition of Vero cells when treated with different concentrations of clarified crude and encapsulated PLGA particles.	223

## LIST OF TABLES

<b>Table No.</b>	<b>Title of the Table</b>	<b>Page No.</b>
Table 2.1	Synergistic interactions of PSMs with antibiotics. (-) denotes not mentioned in the reference paper.	41-44
Table 3.1	List of plants used in the present study.	67-68
Table 3.2	Characterization of the four bacterial isolates.	75
Table 4.1	MIC and FIC index of the different bacterial strains.	110
Table 5.1	List of metabolites present in <i>F. religiosa</i> , and their binding energy obtained from ensemble docking.	148-157
Table 5.2	Binding energy (kJ/mol) of all protein-ligand complexes calculated using MMPBSA method.	184-186
Table 5.3	ADMET properties of the plant metabolites and standards used in MD simulation study.	190-192
Table 6.1	The loading capacity and encapsulation efficiency of PLGA 75:25 and 50:50 loaded with different concentrations of clarified crude.	210

## List of Abbreviations

<b>Abbreviations</b>	<b>Description</b>
MRSA	Methicillin resistant <i>Staphylococcus aureus</i>
MIC	Minimum inhibitory concentration
FICI	Fractional inhibitory concentration index
MDR	Multi-drug resistant
PSM	Plant secondary metabolite
PBP	Penicillin Binding Protein
QS	Quorum Sensing
SAR	Structure Activity Relationship
EO	Essential Oil
WHO	World Health Organization
ADMET	Adsorption, Distribution, Metabolism, Excretion, Toxicity
ESBL	Extended Spectrum beta-lactamase
MD	Molecular dynamics
PDB	Protein Data Bank
RMSD	Root Mean Square Deviation
RMSF	Root Mean Square Fluctuation
SASA	Solvent Accessible Surface Area
R <sub>g</sub>	Radius of Gyration
BE	Binding Energy
ABE	Average Binding Energy
HBO	Hydrogen Bond Occupancy
MMPBSA	Molecular Mechanics Poisson-Boltzmann Surface Area
AAR	Amino acid residue
BSA	Bioavailability score
TLC	Thin layer chromatography
AC-R-H	<i>Acorus calamus</i> rhizome hexane
OD	Optical Density
MTT	3-(4,5-dimethylthiazol-2-yl)-2,5-diphenyl tetrazolium bromide
S-III-BAF	Stage three bioactive fraction
FTIR	Fourier Transform Infrared Spectroscopy
EtBr	Ethidium Bromide
SEM	Scanning Electron Microscopy
PBS	Phosphate Buffer Saline
PI	Propidium Iodide
FAME	Fatty acid methyl ester
DMSO	Dimethyl sulfoxide
ANOVA	Analysis of variance
RFU	Relative Fluorescence Unit
PLGA	Poly (lactic-co-glycolic acid)
AC-H-CC	<i>Acorus calamus</i> hexane clarified crude
PVA	Poly vinyl alcohol
DCM	Dichloromethane
DI water	Deionized water
PDI	Polydispersity index
UV	Ultra-violet
HR-LCMS	High Resolution-Liquid Chromatography Mass Spectrometry

GC-MS	Gas Chromatography Mass Spectrometry
GC-FID	Gas Chromatography-Flame Ionization Detection
DLS	Dynamic Light Scattering